



**HAL**  
open science

## Experimental evidence of the three-dimensional flash-over expansion over a nanosatellite mockup

Yoann Bernard-Gardy, Jean-Charles Matéo-Vélez, François Issac, Julien Jarrige, Gaël Murat, Laurent Garrigues

► **To cite this version:**

Yoann Bernard-Gardy, Jean-Charles Matéo-Vélez, François Issac, Julien Jarrige, Gaël Murat, et al..  
Experimental evidence of the three-dimensional flash-over expansion over a nanosatellite mockup.  
2024. hal-04637182

**HAL Id: hal-04637182**

**<https://hal.science/hal-04637182>**

Preprint submitted on 5 Jul 2024

**HAL** is a multi-disciplinary open access archive for the deposit and dissemination of scientific research documents, whether they are published or not. The documents may come from teaching and research institutions in France or abroad, or from public or private research centers.

L'archive ouverte pluridisciplinaire **HAL**, est destinée au dépôt et à la diffusion de documents scientifiques de niveau recherche, publiés ou non, émanant des établissements d'enseignement et de recherche français ou étrangers, des laboratoires publics ou privés.

## Experimental evidence of the three-dimensional flash-over expansion over a nanosatellite mockup

Y. Bernard-Gardy<sup>1</sup>, J.-C. Matéo-Vélez<sup>2</sup>, F. Issac<sup>3</sup>, J. Jarrige<sup>4</sup> and G. Murat<sup>5</sup>  
*ONERA – The French Aerospace Lab – FR-31055 Toulouse, France*  
and  
L. Garrigues<sup>6</sup>  
*LAPLACE, Université de Toulouse, CNRS – FR-31062 Toulouse, France*

**This paper presents efforts made to improve knowledge around plasma bubble expansion during an electrostatic discharge. Previous work provided characteristics of discharges on a nanosatellite mockup charged using electron gun and VUV lamp. In this work the focus is on a mockup immersed into a low-Earth-orbit representative plasma and on the expansion of the plasma bubble in the three dimensions of space. Especially, the objective was to measure whether the plasma bubble discharged the patches unseen from the cathode spot. Still using embedded measurement electronics for the measurements, the mockup is biased using an external charging circuit.**

### I. Introduction

Space environment leads to surface charging on satellites through complex interactions between particles and matter ([1], [2], [3], [4]). The most severe charging events can lead to electrostatic discharges (ESD) ([5], [6]). Especially, the expansion of the related plasma bubble was investigated along solar panels, following a 2-dimension based model [7]. An ESD occurs when a sufficient differential potential sets up. On nanosatellites, it usually takes place between a dielectric and the conductive satellite structure, as such as between solar panels surface and the structure. This triple point between the conductive structure, the dielectric and the vacuum is called a “triple point”. Due to *Fowler-Nordheim* effect, a potential difference between the dielectric and the structure may cause electron emission. In space, these usual triggering conditions set when the dielectric negative charge is lower than the conductor negative charge, called inverted gradient. Depending on the dielectric potential and its secondary electron emission (SEE) profile, the electron emission from the structure may cause an increase of the electron emission, as the SEE yield can set above 1 and thus, cause an electron avalanche towards the plasma sheath. This part of the ESD is called the *blow-off* and triggers a so-called *cathode spot* from which a cold plasma gushes and expand. This second part is called the flash-over, as the expansion of the plasma results in its propagation around the model.

The blow-off leads to a global discharge of the mockup and raises its frame potential, while the flash-over leads to the discharge of the dielectrics. The energy released by the global process may vary but is sufficient to cause severe damages [8].

From our knowledge, flash-over current waveforms reported in the literature all focus on 2D configurations with a conductive plate supporting an insulating sheet or with solar panel coupons ([9], [10]). The objective of this paper is to demonstrate the ability of the flash-over plasma to generate currents on insulators located all around the satellite, with a 3D expansion allowing to discharge elements not facing the ESD cathode spot. Previous work provided characteristics of discharges on a nanosatellite mockup charged using electron gun and VUV lamp [11]. The present paper focuses on a mockup immersed into a low-Earth-orbit representative plasma and on the expansion of the plasma

---

<sup>1</sup> Yoann Bernard-Gardy, PhD student, Département Physique Instrumentation et Espace, AIAA member grade

<sup>2</sup> Jean-Charles Matéo-Vélez, Research engineer, Département Physique Instrumentation et Espace, AIAA member grade

<sup>3</sup> François Issac, Research engineer, Département Électromagnétisme et Radar, AIAA member grade

<sup>4</sup> Julien Jarrige, Research engineer, Département Physique Instrumentation et Espace, AIAA member grade

<sup>5</sup> Gaël Murat, Technician, Département Physique Instrumentation et Espace, AIAA member grade

<sup>6</sup> Laurent Garrigues, Research director, Groupe de Recherche Énergétique, Plasmas et Hors équilibre, AIAA member grade.

bubble in the three dimensions of space. Section II presents the experimental setup including a parallelepipedic nanosatellite mockup equipped with discharge sensors. The experimental results are presented in Section III. Section IV is a discussion and a conclusion of the work.

## II. Experimental setup

### A. Overview

A nanosat mockup is mounted at the center of a plasma chamber with non-conducting nylon wiring, it embeds a power supply and a measurement electronic board, connected to the laboratory acquisition system through optic fibers described in [11]. The test facility used for these experiments is the JONAS plasma tank located at ONERA Toulouse Center. It is a 3.4 m long cylinder 1.85 m in diameter equipped with an electron gun, a UV source and a plasma source [12]. During previous experiments, an electron beam was used to charge the mockup down to a few hundreds or thousands of volts negative and a VUV lamp was used to induce a positive differential charging on dielectrics through the photoemission of electrons. The objective of the present paper, i.e. assessing the flashover ability to neutralize the dielectrics on the entire mockup surface, makes it inconvenient to use unidirectional impinging fluxes of charging particles. Both the electron beam and the VUV source are inefficient at charging surfaces not directed towards the irradiation source. To charge the insulators on all directions, it is chosen to use a plasma source to neutralize the insulating covers with respect to the chamber walls. This results in the positive differential charging of the insulators with respect to the negatively charged nanosatellite structure, thus reproducing the inverted gradient situation. However, the use of plasma leads to a pressure of  $10^{-5} mbar$  in the JONAS chamber, which prevents the use of the electron gun because of possible damage of the electron emitting hot wire. To obtain a negatively charged frame potential, the structure of the nanosatellite mockup is biased with an external negative voltage supply.

Figure 1 shows the mockup installation in the JONAS chamber and defines the axis reference frame. The plasma source is directed from the -X to the +X direction.

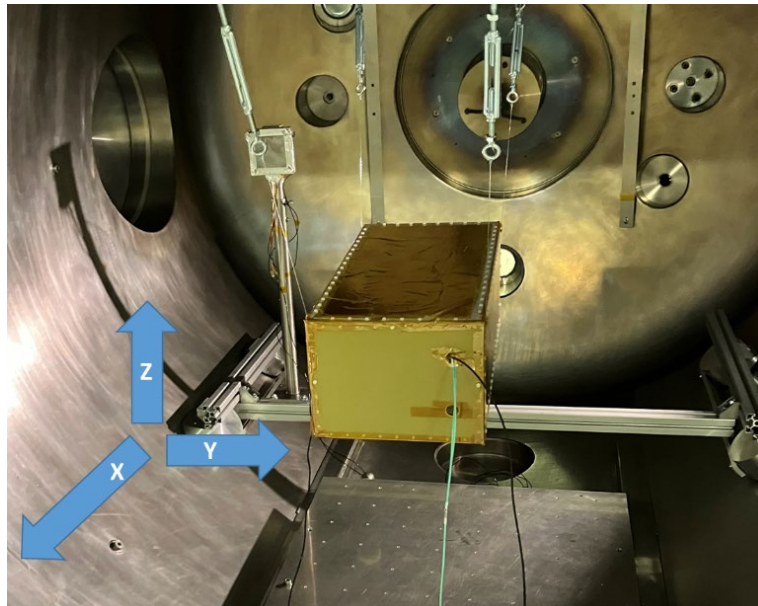


Figure 1 - Mockup installation in JONAS chamber. The mockup is attached to the tank with insulated wires.

## B. Nanosatellite mockup

The model is a 15U-like nanosat, measuring 40 cm x 20 cm x 15 cm in the X, Y and Z directions, respectively. It is based on an aluminium frame on which six panels are fixed, using non-conducting Teflon screws. These panels are raw printed circuit board (PCB) with a copper layer on the internal side. The outer side of the 5 panels located in the -X, +/-Y and +/- Z directions is a copper layer. The internal sides are electrically connected to the aluminum structure. The external side of each panel is divided in several patches and covered with a 12.5  $\mu\text{m}$ -thick Kapton® layer, except the +X-direction panel, which is made of epoxy. The Kapton layers completely overlap the copper conductors. No adhesive is used to fix the insulating sheets. They adhere to the PCB external face only by electrostatic forces. Each patch is grounded to the frame with a wire passing through the PCB with a via. Figure 2 shows the -X face which consists in a rectangular board with two concentric circles. A square hole is performed at the center of the Kapton® covering sheet and a specific component is introduced inside the hole. This component consists in a series of triple point configurations. Two triple point configurations have been tested. During the first part of the experiment, a circular hole 15 mm-large was performed to let appear a piece of aluminum scotch, overlapped by strips of 3mm-wide 25 $\mu\text{m}$ -thick Kapton® tape, as shown in Figure 3. During the second part of the experiment, eight 3mm-wide 25  $\mu\text{m}$ -thick strips equally separated recover the 30 mm-side square aluminium scotch patch, leading to 8 gaps, each 0.6 mm wide shown in Figure 4. The objective of this setup is to control the location of the ESD onset at the center of patch A.

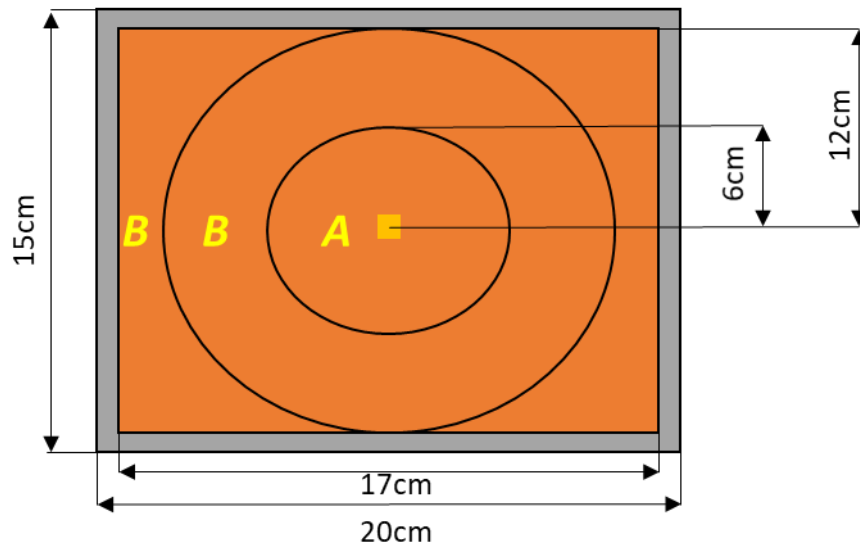
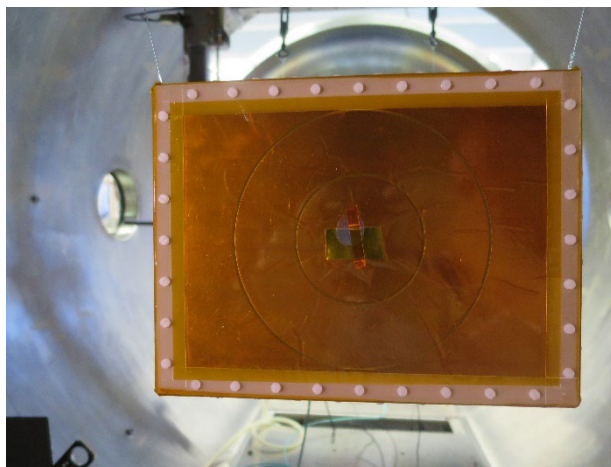
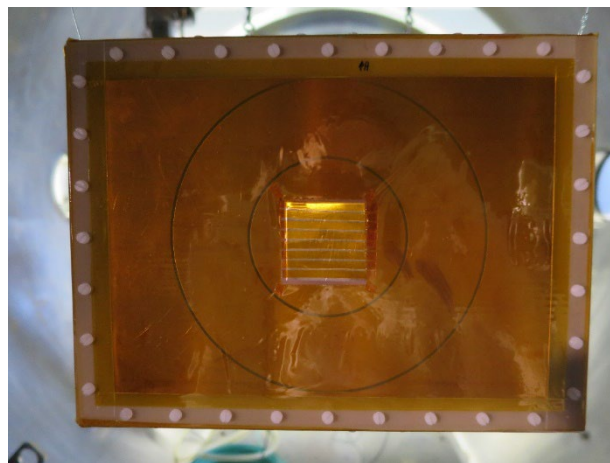


Figure 2 - mockup -X face, facing plasma. The square in the middle of patch A represents the hole in the insulating covering sheet. The yellow letters are the measurement channels to which the patches are connected.



**Figure 3 – First triple point configuration made of an aluminium patch overlapped with a 3 mm-wide Kapton® tape.**



**Figure 4 – Second triple point configuration made of a 30mm-side square aluminium patch covered with 3mm-wide Kapton® tape strips**

The  $\pm Y$  and  $\pm Z$  panels, named side panels in this paper, are similar to one another. They consist in a rectangular board split in 5 rectangular sectors. The size of each sector is presented in Figure 5. The  $+X$  panel is a raw PCB board without conductor. No measurement is performed on that panel. It is used to pass wiring from the tank wall to the equipment located inside the mockup.

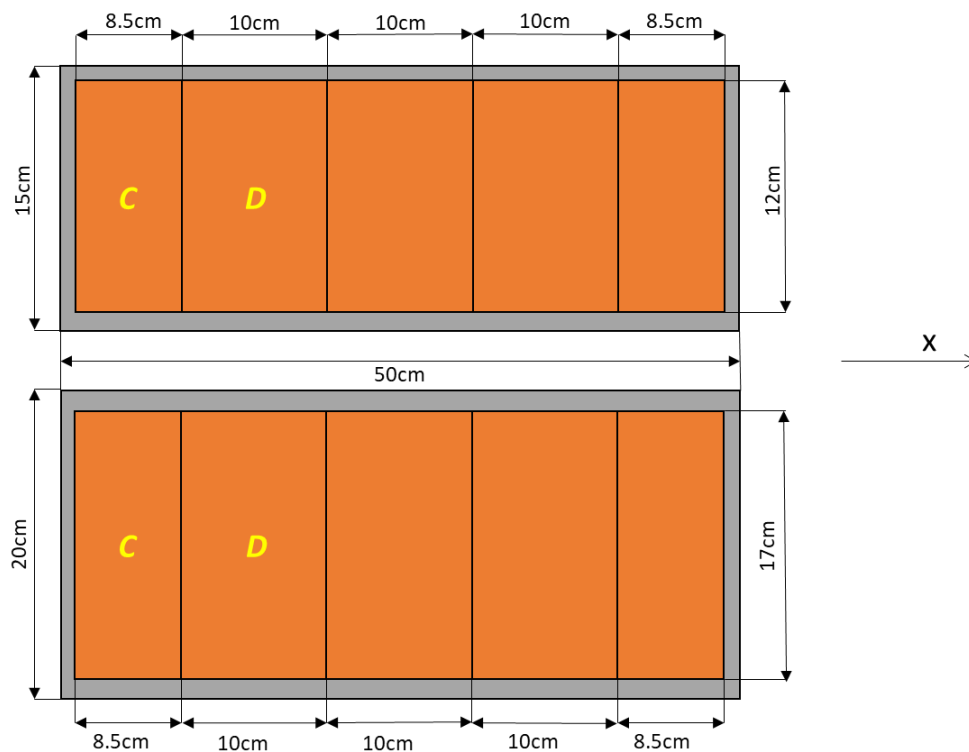


**Figure 5 -  $\pm Z$  faces and  $\pm Y$  faces, respectively from top to bottom. The yellow letters are the measurement channel to which the patch is connected**

### C. Instrumentation

The mockup embeds measurement electronics and connection to the data acquisition computer through insulated optical fiber. A battery and a power supply are mounted in the mockup to feed the instruments from the inside. An oscilloscope is used to digitalize the outputs of transient current sensors. The sensors are Pearson® current probes (ref 2877) with a bandwidth of 100 MHz. The probes are mounted on the wires that connect the panel patches to the mockup frame according to the diagram of Figure 6 representing the mechanical and electrical connections in the mockup and to the oscilloscope channels identified in Figure 5.

All measurements are performed with a  $50 \Omega$  load on the oscilloscope entry channels to reduce fast transient reflection. The measurement chain gain is  $0.5 \text{ V/A}$ . The signal is digitalized with a rate of  $200 \text{ MS/s}$ . To meet Shannon-Nyquist criteria, a  $98 \text{ MHz}$  filter is placed at the oscilloscope entries.

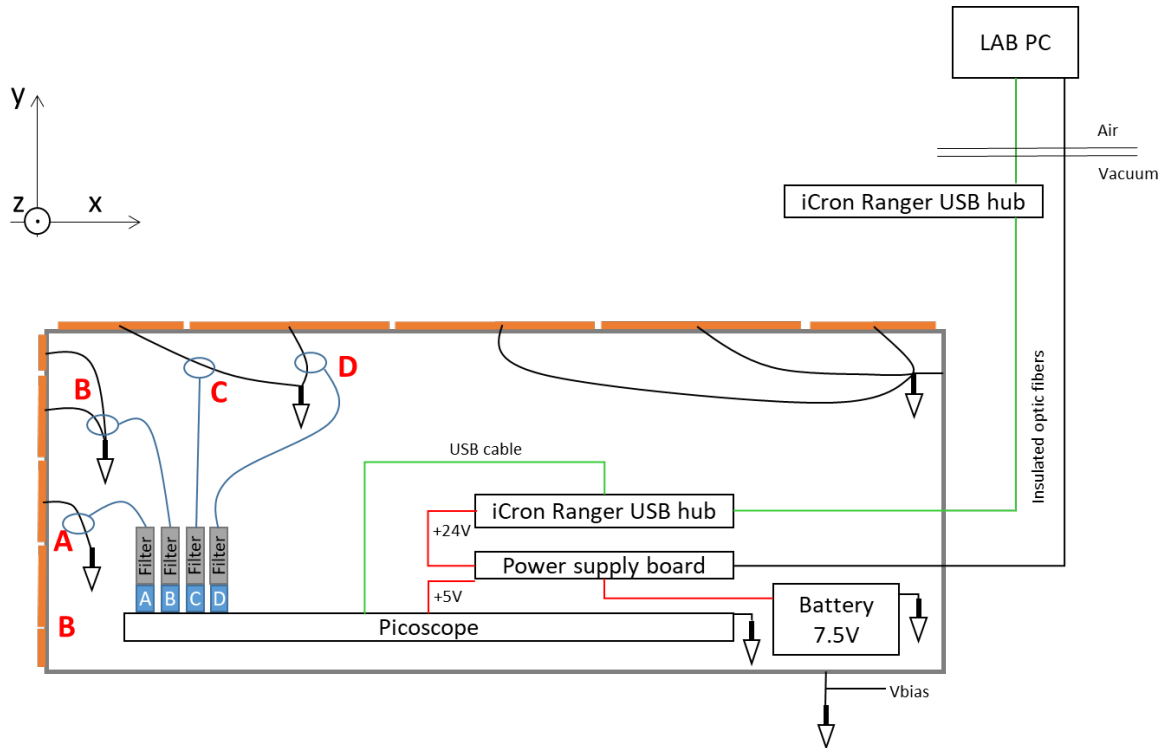


Figure 6 –Instrumentation of the nanosatellite mockup. White arrows represent the structure ground. Letters in red indicate which oscilloscope channels the patches are connected to.

### D. Charging conditions

Figure 7 schematically represents the mockup installed in the JONAS chamber. The plasma source generates  $\text{Ar}^+$  ions of a few eV temperature, a drift velocity of around  $10 \text{ km/s}$  and a density of  $10^{11} \text{ part} \cdot \text{m}^{-3}$  to  $10^{12} \text{ part} \cdot \text{m}^{-3}$ . The plasma source is located at a distance of  $1.6 \text{ m}$  from the  $-X$  panel. The mockup is negatively biased to a potential  $V_{bias}$  with respect to the tank walls thanks to a high voltage power supply connected to a capacitor  $C_{bias}$  of  $100 \text{ pF}$  through a resistor of  $56 \text{ k}\Omega$ . The total charge stored in the structure of the mockup, which is available for the blow-off current, is  $Q_{BO} = (C_{bias} + C_{sat}) \cdot V_{bias}$  where  $C_{sat}$  is the capacitance of the satellite with respect to the plasma sheath boundary. Assuming the capacitance of sphere in vacuum is  $4 * \pi * \epsilon_0 * r$  where  $r = 0.25 \text{ m}$  which is equivalent radius of the mockup,  $C_{sat} \approx 9 \text{ pF}$ . And assuming a Debye length  $\lambda_D$  of a few centimetres, the capacitance is rather

described by the 2D planar capacitor model:  $\epsilon_0 * S / \lambda_D$  with S the surface of the mockup, which leads to  $C_{sat} \approx 350pF$ .

The mockup voltage is measured with a high voltage probe with an input impedance of 500 M $\Omega$ . The transient current flowing through  $C_{bias}$  is measured with a Pearson® probe 4722.

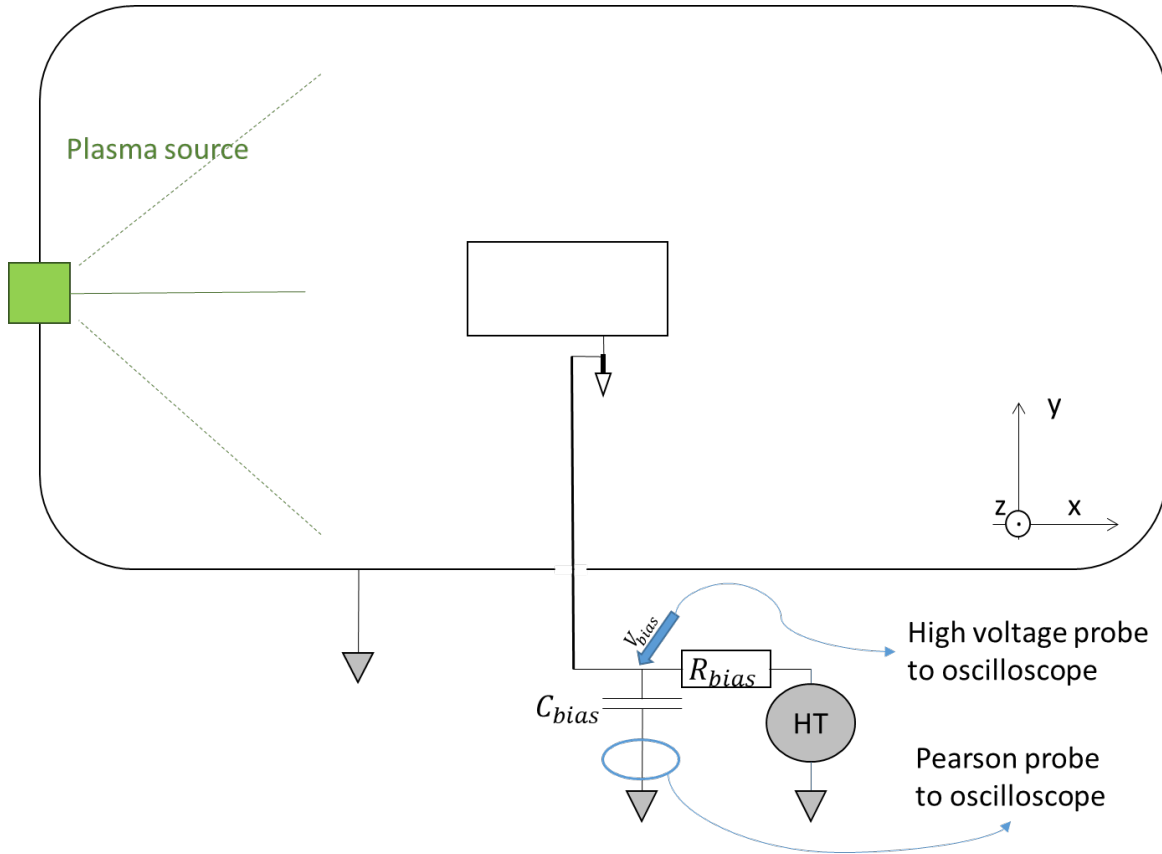


Figure 7 – JONAS chamber test setup. Grey and white arrows stand for laboratory and mockup structure grounds, respectively

## E. Current paths

The current monitored by channel A flows through the wire connected to the triple point of the mockup. As this point is the siege of the cathode spot, the measured current integrates both blow-off and flash over currents.

The cathode spot and the plasma bubbles carry the current during the dielectrics discharge, which correspond to the flash-over. Thus, when the plasma bubble expands and reaches a dielectric, the electrons facing the charged dielectrics and located on the conductive patch move along the structure up to the cathode spot and close the loop. The plasma bubble fully or partially discharges the dielectric surfaces, depending on their position and on the duration of the cathode spot. The Pearson probe instrumenting the corresponding patches, monitors this displacement current and so for the one related to channel A.

Figure 8 schematically represents the plasma bubble expansion and the current paths.

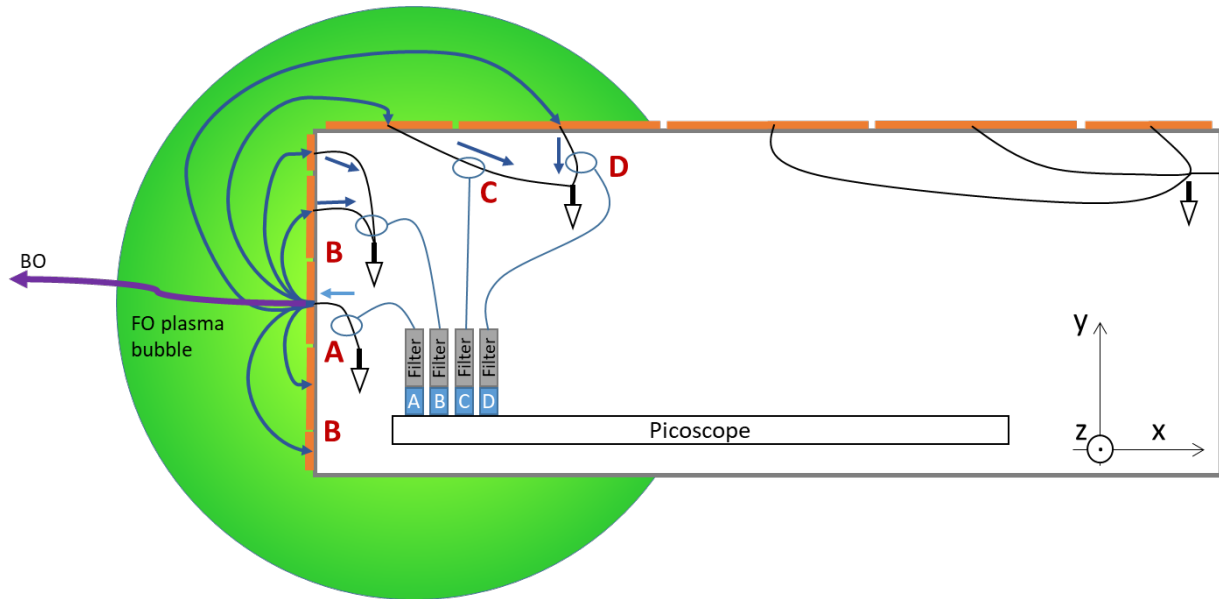


Figure 8 – Current path during plasma bubble expansion.

### III. Results

A number of 55 ESD have been registered. Their duration ranges from 10 to 40  $\mu\text{s}$ , with an average of 20  $\mu\text{s}$ . The current peak on main channel A reaches up to 4 A, with an average between 1.5 A and 2 A. The mockup bias potential varied from - 400 to - 750 V. 19 out of 55 ESDs have been discarded from the post-processing routine because of the unreliability of the measurements. The most common reason is the saturation of a measurement channels.

#### A. Typical results

Figure 9 and Figure 10 show the current and bias voltage waveforms obtained with ESD 12 and ESD 39, respectively in the first and second triple point configuration. The measurement on channels A to D are compared to the time evolution of the mockup bias voltage and to the current flowing through  $C_{bias}$ . Most waveforms are similar in shape and duration to that of ESD 12 and ESD 39, regardless of the bias voltage. The bias voltage applied to the mockup was - 700 V from ESD 1 to 19 with the first triple point configuration and - 400 V to -450 V from ESD 20 to 55 with the second triple point configuration. There is no significant effect of the triple point configuration and applied bias voltage on the peak current and flash-over duration.

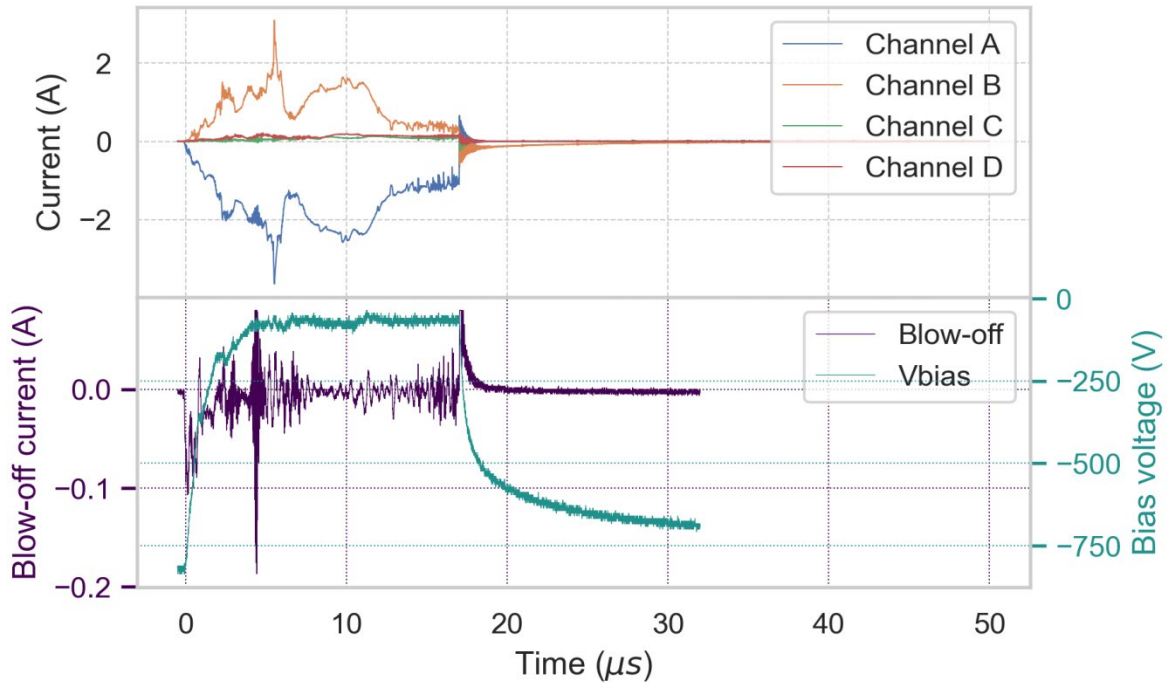


**Figure 9 – Current measurements on (top) the mockup and (bottom) on the charging circuit during ESD12 with  $V_{bias} = -750V$ .**

Figure 9 presents the currents measured by the embedded electronics on the four measurement loops. It also presents the blow-off current and  $V_{bias}$  voltage measured by the Pearson probe located between the capacitor and the charging circuit and by the high voltage probe, respectively. The blow-off current reaches a value of 0.1 A after 0.5  $\mu s$  and then quickly oscillates between smaller values. Dissipated charge is about 100nC. This blow-off current discharges the mockup structure down to  $-100 V$  within 2.5  $\mu s$ . The mockup potential remains almost constant until the end of the discharge at  $t = 18 \mu s$ .

Channel A measures the electron current from the mockup structure to the cathode spot. Measured current is negative, indicating that electrons are flowing from the mockup to the vacuum chamber. Part of this current is composed of blow-off current, as the other part is the flash-over current, reaching other patches (B, C, D and the ones uninstrumented) with a maximal value of 3.5 A for ESD 12. Both blow-off and flash-over currents are measured on Channel A. The dissipated charge through the cathodic spot is  $28 \mu C$ , which is significantly higher than  $Q_{sat} = C_{sat} \cdot V_{bias} < 1 \mu C$ . This means that the flash-over current dissipates a much larger amount of charge than the blow-off. The capacitance of all of the dielectrics combined  $C_{diel}$  is about 500nF, which means  $C_{diel} + C_{sat} \approx C_{diel}$ . The theoretical differential charge stored within dielectrics all over the mockup is about  $350 \mu C$ , meaning that the surface of the covering dielectrics is not fully discharged at the end of the ESD.

The current on Channel B is almost the opposite of that measured in channel A. From the current paths indicated in Figure 8 it means that the main contributor to the flashover is coming from the surfaces the closest to the cathode spot. The current is looping as expected, through the plasma bubble.

Channels C and D exhibit less significant but noticeable currents, of about 0.1 A and 0.2 A respectively, with the same duration. This proves that flash-over current can loop over surfaces not in direct sight from the cathode spot.

Cathode spot allow blow-off and flash-over currents existence. When it stops, both currents come to an end. At 18  $\mu s$ , the discharge stops, charging current reaches 0.05A and bias voltage slowly return to its nominal value in few microseconds. This is consistent with an RC-circuit characteristic time of  $R_{bias} * C_{bias} = 5 \cdot 10^4 \times 10^{-10} = 5 \mu s$ .

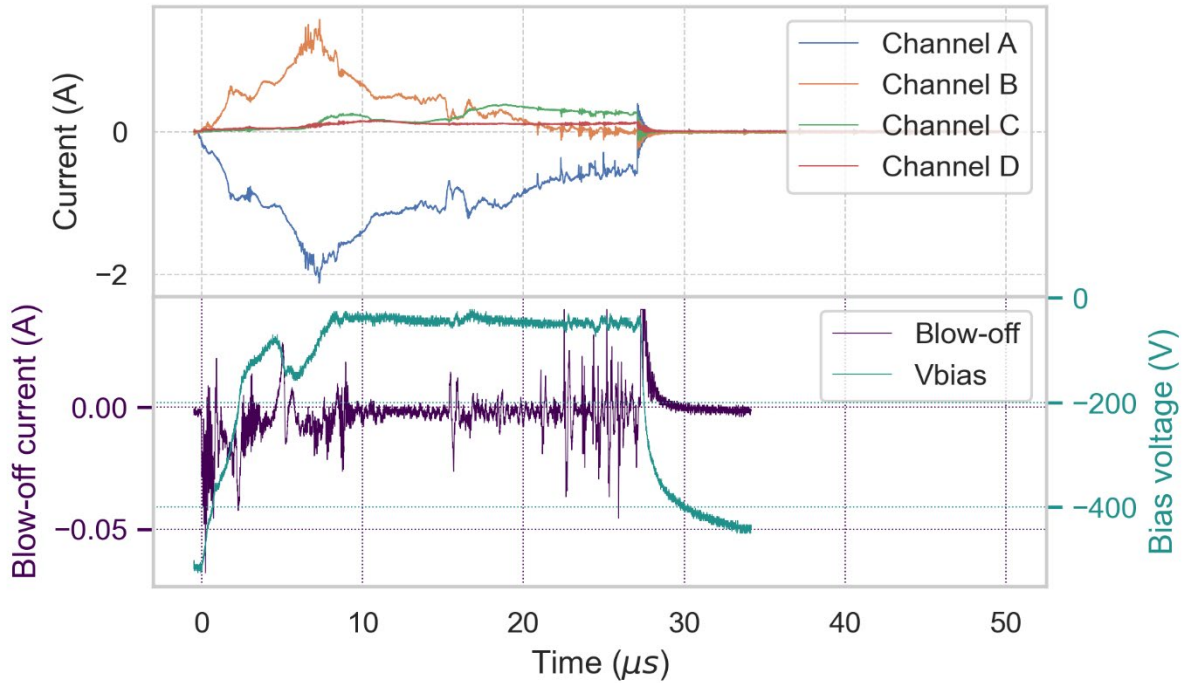


**Figure 10 – Current measurements on (top) the mockup and (bottom) on the charging circuit during ESD39 with  $V_{bias} = -450V$ .**

The waveforms of ESD 39 with the second triple point configuration, presented in Figure 10, have the same overall shape to that presented in Figure 9. We observed no significant change in the waveforms regardless of the triple point configuration.

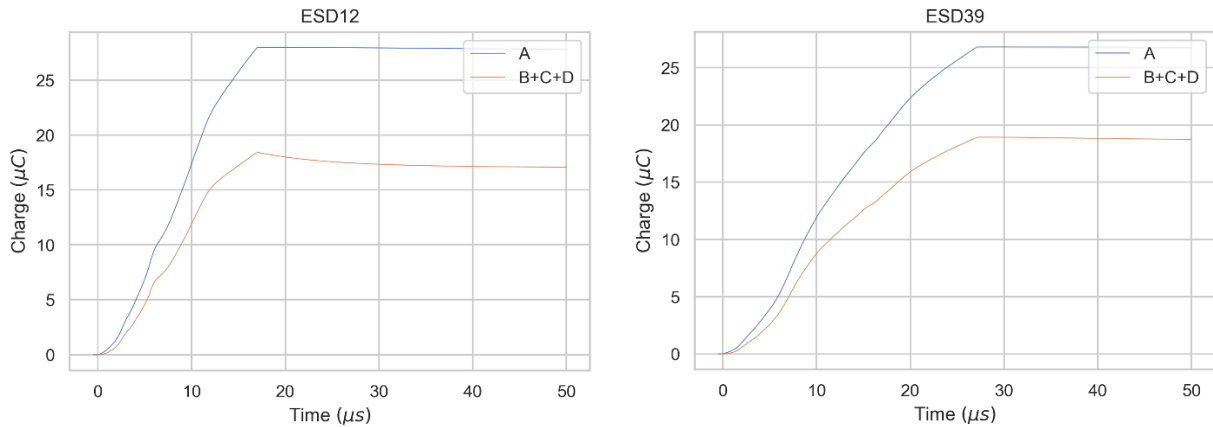


**Figure 11 – Cumulated charge measured on Channel A and on Channels B, C and D for (left) ESD 12 and (right) ESD 39.**

Figure 11 shows the time evolution of the cumulated charge dissipated through Channel A and through the sum of the other channels (B, C and D) for ESD 12 and ESD 39. The overall dissipated charge on channel A ranges between 26 and 27  $\mu C$  for both ESDs, while the overall dissipated charge on the three other channels ranges between 17 and 19  $\mu C$ . The dissipated charge on channels B, C and D is around 30 % lower than that dissipated on channel A. It suggests that the flash-over also involve non-instrumented patches.

## B. ESD main characteristics

Figure 12 shows the total charge dissipated on each instrumented patch for all ESDs.  $Q_A$ ,  $Q_B$ ,  $Q_C$ ,  $Q_D$  are the charges dissipated on patches A, B, C and D respectively.  $Q_O$  is the charge dissipated on the non-instrumented patches and  $Q_{BO}$  is the charge stored in  $C_{bias} + C_{sat}$ . Following to the electrical circuit presented in Figure 8,  $Q_A$  is the sum of  $Q_B$ ,  $Q_C$ ,  $Q_D$ ,  $Q_O$  and  $Q_{BO}$ . It ranges from 10 to 50  $\mu\text{C}$  for the 35 ESD. The highest values are obtained with the first triple point configuration, probably because it used a larger bias voltage than the second triple point configuration.

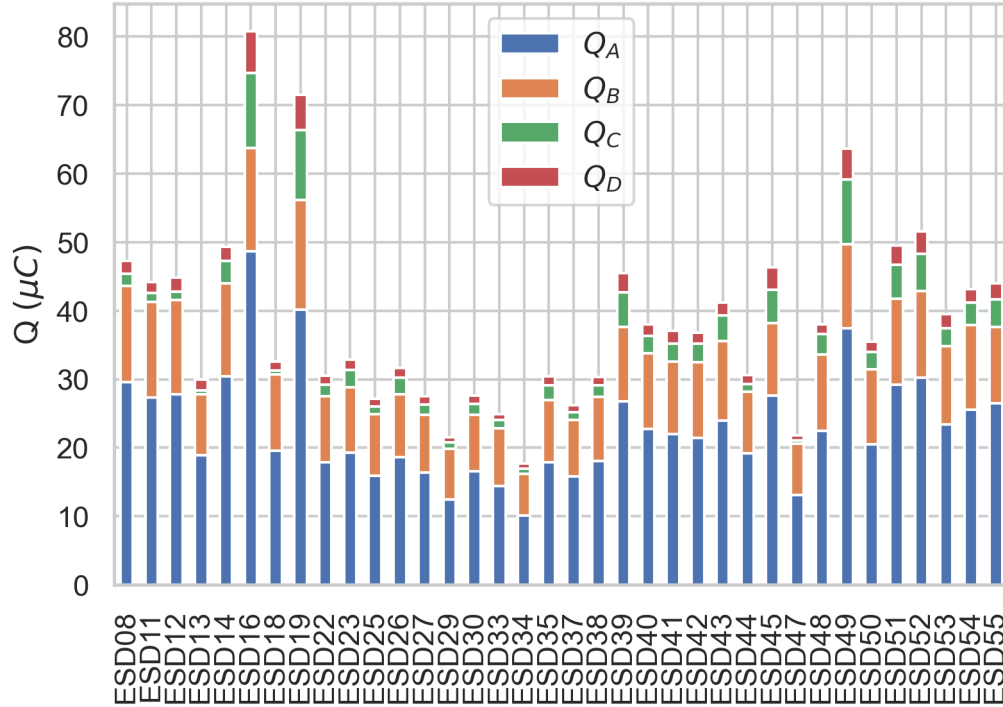


Figure 12 – Overview of measured charge for each channel, stacked per ESD.

Figure 13 **Erreur ! Source du renvoi introuvable.** shows the ratio between  $Q_B + Q_C + Q_D + C_{sat} \cdot V_{bias}$  and  $Q_A$ . This ratio is less than one, indicating that part of the current flowing through A is not flowing through the other instrumented patches.

Considering the mockup geometry of the side panels, the total of dielectric area on all the side panels is  $S_{side} = 2 \cdot S_C + 3 \cdot S_D$ , where  $S_C, S_D$  stand for the surface associated with channel C and D respectively. Assuming a linear relationship between the dissipated charge and the surface of the insulating patches [13], a corrected ratio is also given in **Erreur ! Source du renvoi introuvable.**, i.e. the ratio between  $Q_B + 2 \cdot Q_C + 3 \cdot Q_D + C_{sat} \cdot V_{bias}$  and  $Q_A$ . This ratio is closer to one.

The total measured charge is lower than the available charge. Indeed, the theoretical charge stored on insulating covers is  $221\mu\text{C}$  and  $344\mu\text{C}$  for a bias voltage of  $-450\text{ V}$  and  $-700\text{ V}$  respectively. It suggests that the flash-over produced within the frame of these experiments does not fully discharge the dielectrics.

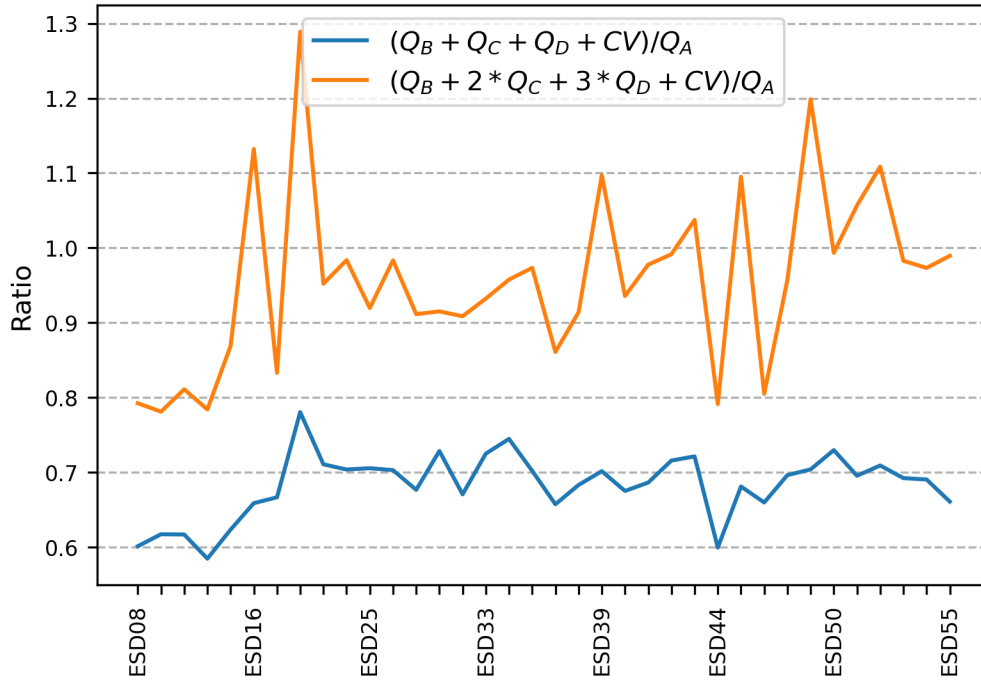


Figure 13 – Comparison between measured charge on channel A with blow-off charge and both measured (blue) and extrapolated (orange) flash-over.

The plotting of a smooth distribution of all these measurements, normalized towards the dissipated charge at the cathode spot, i.e. channel A measured charge, is shown on Figure 14. This kernel density estimate (KDE) plot smooths the discrete results into the continuous domain using a Gaussian kernel and producing a continuous density estimate [14].

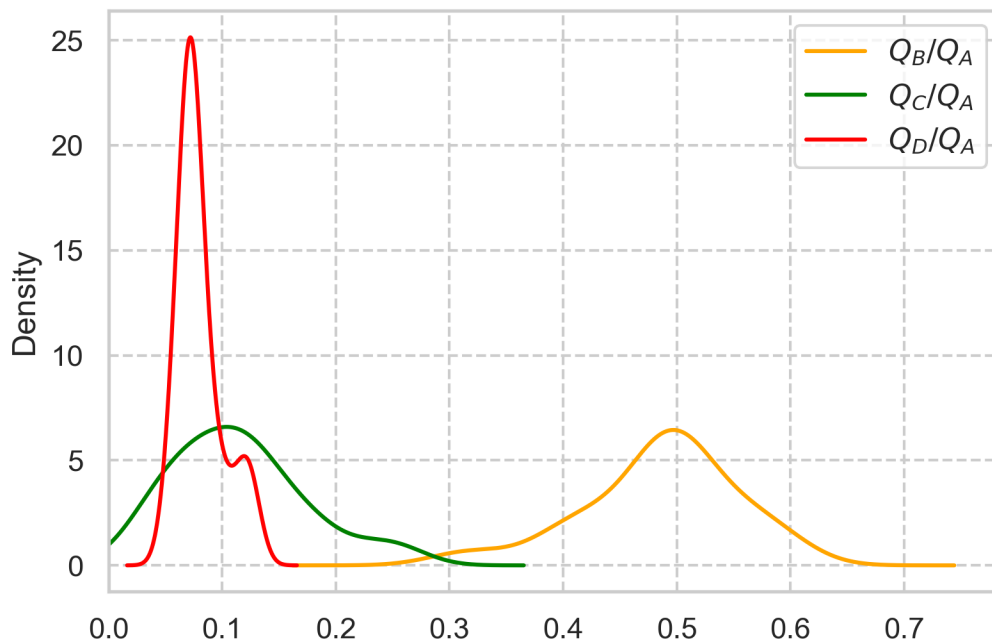
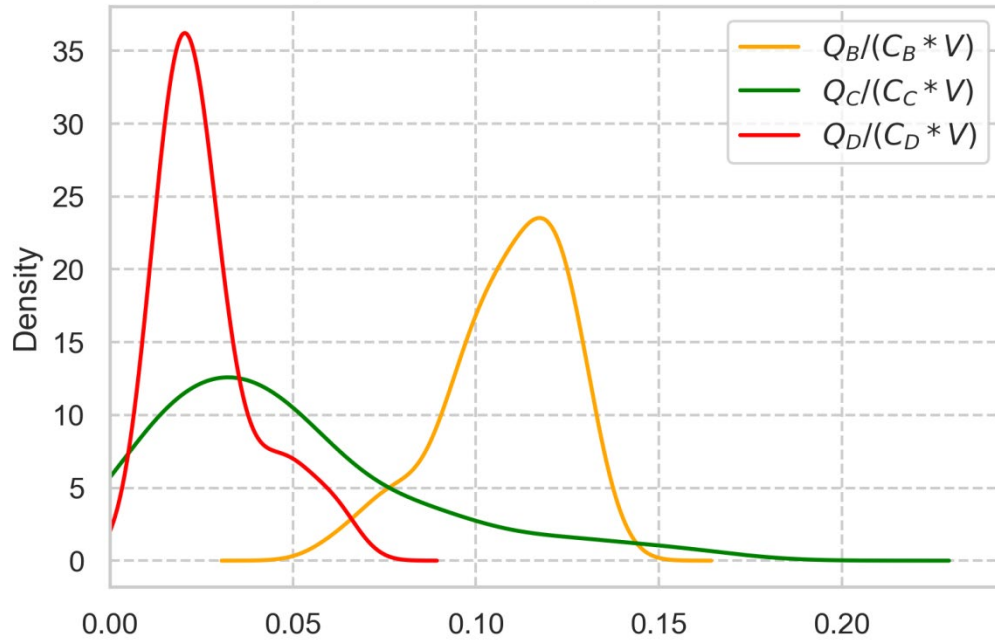


Figure 14 – Kernel density estimation plot of measured charge per loop, normalized over the A channel.

The distribution of  $Q_B$  sets up around 50 % of  $Q_A$ , with a standard deviation of 7 %, while these values for  $Q_C$  and  $Q_D$  are respectively 10 % ( $\sigma_C = 6 \%$ ) and 8 % ( $\sigma_D = 2 \%$ ).

The same kind of information is also extracted from the experimental data, using not the dissipated charge on the cathode spot as the normalization number but the available charge in the dielectric related to the measured channel. This graph is presented in Figure 15.



**Figure 15 – Kernel density estimation plot of the measured charge per channel, normalized over the charge available on the corresponding surface.**

It appears that the dielectrics are not entirely discharged, which confirms previous observations. Figure 15 shows that in average, dissipated charges represent 12 %, 3 % and 2 % of the available charge stored at the surface of the corresponding surfaces for the channels B, C and D respectively. The farther from the cathode spot, the weaker the percentage of charge dissipated.

#### IV. Conclusion

Work and conclusions exposed in this paper form a preliminary step in the understanding of 3D plasma bubble expansion around a charged object in a plasma environment.

During this experiment on a nanosatellite mockup, flash-over currents have been measured on panels hidden from the cathode spot. This implies that during an ESD, the plasma bubble expands all around the surface and the discharge current loops through it. The current amplitude decreases with the distance from the cathode spot. However, the duration is the same for all the instrumented patches. In average, about 10% of the charge initially stored on the dielectrics is dissipated during the flash-over for patches in the same plane and less than 5% for those in orthogonal planes.

The step following this work is to instrument all the patches simultaneously. This implies the addition of another embedded electronic measurement board, to increase the number of measurements.

## V. Acknowledgments

This work was performed in the frame of the ONSAT-1 program of ONERA.

## VI. References

- [1] M. Cho, *Charging and Discharge in Vacuum and Space*, 2007 IEEE International Vacuum Electronics Conference, Kitakyushu, Japan, 2007, pp. 1-4, doi: 10.1109/IVELEC.2007.4283197.
- [2] Vayner, Boria & Galofaro, J. & Ferguson, Dale & de Groot, Wilhelmus. (2002). Electrostatic Discharge Inception on a High-Voltage Solar Array. 40th AIAA Aerospace Sciences Meeting and Exhibit. 10.2514/6.2002-631.
- [3] D. E. Hastings and H. B. Garrett, *Spacecraft-Environment Interactions*, Cambridge Atmospheric and Space Science Series, Cambridge University Press, 1996, 10.1017/CBO9780511525032.
- [4] H.B. Garrett and A.C. Whittlesey, *Guide to Mitigating Spacecraft Charging Effects* (Wiley, Hoboken, 2012), 10.1002/9781118241400.
- [5] Fennell, J. F., Koons, H. C., Roeder, J. L., and Blake, J. B., "Spacecraft Charging: Observations and Relationship to Satellite Anomalies," Aerospace Corp. TR 2001(8570)-5, El Segundo, CA, Aug. 2001, <https://apps.dtic.mil/sti/citations/ADA394826> [retrieved 10 July 2022]
- [6] Anderson, P. C., and Koons, H. C., "Spacecraft Charging Anomaly on a Low-Altitude Satellite in an Aurora," *Journal of Spacecraft and Rockets*, Vol. 33, No. 5, May 1996, pp. 734–738.
- [7] L. Monnin, S. L. G. Hess, J.-F. Roussel, P. Sarrailh, and D. Payan, "Flash-over propagation simulation upon spacecrafts solar panels", *J. Appl. Phys.* 130, 223302 (2021), 10.1063/5.0061320.
- [8] Ahmad, N., Herdiwijaya, D., Djamaluddin, T., Usui, H., and Miyake, Y., "Diagnosing Low Earth Orbit Satellite Anomalies Using NOAA-15 Electron Data Associated with Geomagnetic Perturbations," *Earth Planet Space*, Vol. 70, No. 91, 2018, pp. 1343–8832.
- [9] J. A. Young and M. W. Crofton, "ESD Propagation Dynamics on a Radially Symmetric Coupon," in *IEEE Transactions on Plasma Science*, vol. 43, no. 10, pp. 3749-3759, Oct. 2015, doi: 10.1109/TPS.2015.2475719
- [10] J. A. Young and M. W. Crofton, "The Effects of Material at Arc Site on ESD Propagation," in *IEEE Transactions on Plasma Science*, vol. 45, no. 12, pp. 3349-3355, Dec. 2017, doi: 10.1109/TPS.2017.2765244
- [11] Bernard-Gardy, Y., Matéo-Vélez, J. C., Issac, F., Jarrige, J., Murat, G., Garrigues, L., & Payan, D. (2023). *Innovative technique for electrostatic discharges characterization on a floating nanosatellite mockup*. *Journal of Spacecraft and Rockets*, 60(1), 172-180.
- [12] J.C. Matéo Vélez, J.-F. Roussel, D. Sarrail, F. Boulay, V. Inguibert, and D. Payan. Ground plasma tank modelling and comparison to measurements. *IEEE Transactions on Plasma Science*, 36(5):2369–2377, October 2008.
- [13] J. -C. Matéo-Vélez et al., "Development of an Experimental Instrumentation Dedicated to ESD Testing and Measurement on Nanosatellites," in *IEEE Transactions on Plasma Science*, vol. 51, no. 9, pp. 2544-2549, Sept. 2023, doi: 10.1109/TPS.2023.3262354.
- [14] <https://seaborn.pydata.org/tutorial/distributions.html#tutorial-kde> accessed on the 1<sup>st</sup> of may, 2024.